Reducing Interface Recombination through Mixed Nanocrystal Interlayers in PbS Quantum Dot Solar Cells

Santanu Pradhan[1], Alexandros Stavrinadis[1], Shuchi Gupta[1], and Gerasimos Konstantatos[1, 2]*

[1] ICFO-Institut de Ciencies Fotoniques, The Barcelona Institute of Science and Technology, 08860 Castelldefels (Barcelona), Spain

[2] ICREA—Institució Catalana de Recerca i Estudis Avançats, Passeig Lluís Companys 23, 08010 Barcelona, Spain

* gerasimos.konstantatos@icfo.es

Abstract: The performance of ZnO/ PbS colloidal quantum dot (CQD) based heterojunction solar cells is hindered by charge carrier recombination at the heterojunction interface. Reducing interfacial recombination can improve charge collection and the photocurrent of the device. Here we report the use of a mixed nanocrystal (MNC) buffer layer comprising zinc oxide nanocrystals and lead sulfide quantum dots at the respective heterojunction interface. Remote trap passivation of the PbS CQDs taking place within this MNC layer reduces interfacial recombination, electron back transfer and improves charge collection efficiency. Upon the addition of the MNC layer, the overall power conversion efficiency increases from 9.11% to 10.16% and Short-circuit current density (J_{SC}) increases from 23.54 mA/cm^2 to 25.23 mA/cm^2. Optoelectronic characterization of the solar cells confirms that the effects underlying device improvement are reduced trap density and improved charge collection efficiency due to the presence of the MNC buffer layer.

Keywords: colloidal quantum dots, PbS, interface recombination, photovoltaics, mixed nanocrystals

Introduction:

Solution processed colloidal quantum dot (CQD) based photovoltaics (PV) have attracted significant research interest due to the advantages of low-cost solution processibility and optical properties tunability of CQDs[1-3]. In particular, rapid progress made in ZnO/ PbS CQD based solar cells has been facilitated by optimizing device architectures[4], understanding the device physics[5] and improving the electronic properties and surface passivation of QD films and devices[6, 7]. As a result, the power conversion efficiency (PCE) of CQD solar cells improved from 1% to over 11% in the last decade [8, 9].

In spite of this tremendous progress, further improvements to suppress the various loss mechanisms that hinder the performance of these devices is still in search. Such a loss mechanism is the undesired interface recombination of photo-generated charge carriers. While non-radiative recombination in the PbS QD solids plays a major role in the open circuit voltage (V_{OC}) deficit[10-12], interfacial recombination at the ZnO/ PbS heterojunction influences the charge collection and hence the PCE[13]. High efficiency PbS quantum dot solar cells are based on a depleted heterojunction formed between the transparent n-type ZnO layer and the photo-absorbing p-type (with respect to ZnO doping) PbS QD layer. Electron collection at the transparent electrode depends on the efficient electron transfer from PbS to ZnO and reduction of electron back transfer from ZnO to PbS. The latter is even more relevant when the solar cell is operated under realistic conditions in the maximum power point. Efficient electron transfer from PbS to the ZnO depends on the rate of charge transfer and the rate of interface recombination[14]. It is thus important to improve the charge transfer rate and decrease interfacial recombination for improved charge collection, particularly under maximum power point (MPP) operation. The reduction of the interfacial charge carrier recombination can be achieved via the reduction of interfacial charge carrier density and recombination velocity[15]. These parameters are influenced by the presence of defects in ZnO located in the vicinity of the

junction. Suppressing these defects can reduce the interfacial recombination and hence can enhance charge collection at the electrode.

In the past, several techniques have been adopted to reduce the charge carrier recombination at the interface. For TiO_2/PbS solar cells, a thin ZnO layer over TiO_2 has been reported as an efficient buffer layer for reducing interface recombination[16]. Yuan et. al. showed that n-type PCBM ([6,6]-phenyl-61-butyric acid) can be an efficient buffer layer to replace the ZnO layer as it energetically fits in between the n-type and p-type layer of the heterojunction[17]. Doped ZnO has also been presented as an efficient buffer layer[18] which changes favourably the n-type doping concentration at the electron accepting side of the device[19]. Recently, Zhao et. al. have demonstrated a CdSe buffer layer in PbS QD solar cell following the well-known CIGS solar cell buffer layer approach where band bending energetically helping in the smooth conduction of electron from PbS to ZnO[20]. Overall, an ideal interfacial buffer layer must be trap-free, nearly intrinsic as well as energetically favourable to fit in between ZnO and PbS, and such layer had thus far remained elusive. Instead of relying on the employment of other materials, in this work we report the use of a mixed nanocrystalline (MNC) layer comprising ZnO nanocrystals (NCs) and PbS CQDs i.e. the individual components of the heterojunction as a buffer layer that fulfils the aforementioned desired characteristics. Such a mixed nanocrystalline composite has been reported in the past to act as a nearly trap free material when used as a bulk heterojunction quantum dot layer [21, 22], achieving very high V_{OC} and approaching the band-to-band recombination regime.

The MNC layer is prepared using an optimized mixing weight ratio of PbS and ZnO of 2:1 (details in experimental section of supporting information). The buffer layer was treated with MPA (3-mercaptopropionic acid, 5% in methanol) solution similar to the previous report[21]. To investigate the effect of the MNC layer as a buffer layer, we have compared the MNC-buffer-layer device with the reference solar cell where the active layer PbS QDs are

treated with 1-ethyl-3-methylimidazolium iodide (EMII) and the top electron blocking layer is treated with 1, 2 ethane dithiol (EDT) [23].

Results & Discussions:

Figure 1(a) is a schematic of the respective energy band alignment in short-circuit condition with the presence of MNC buffer layer. The buffer layer helps in electron transport with a favourable energy landscape along with a reduced trap state density and electron back transfer from ZnO to the PbS main absorber. The optimized thickness of the buffer layer is found to be 10 nm (1 layer). Supporting Figure S1 shows the effect of thickness variation of MNC buffer layer on the device performance compared to the reference device. Increasing the thickness of the MNC layer from 10 to 40 nm decreases gradually the PCE of the devices. The major reason for this decrement is associated with the decrease of both short circuit current density (J_{SC}) and fill factor (FF). The FF is highly influenced by the increase of series resistance (R_s) upon increasing the thickness of the MNC layer. Interestingly, the open circuit voltage (V_{OC}) of the devices with the MNC layer improved slightly. This indicates that the MNC buffer layer facilitates the decrease interface charge recombination. The thickness of the EMII treated layer for both the devices was approximately 180-190 nm and the EDT layer thickness was close to 30-35 nm whereas the thickness of the ZnO layer was approximately 50 nm. The FIB SEM (scanning electron microscopy) figures for devices with and without the MNC buffer layer are shown in Supporting Figure S2.

The efficiency of the solar cells are estimated from the current density-voltage (J-V) plot as depicted in Figure 1(b). Table 1 summarises the photovoltaic figures of merits for the reference and the MNC buffer layer containing devices. The incorporation of the MNC layer improves J_{SC} from 23.54 mA/cm^2 to 25.23 mA/cm^2 whereas the V_{OC} (0.6 V to 0.61 V) and FF (0.65 to 0.66) also improved slightly. Overall, the PCE improves from 8.80±0.24 % to

9.87±0.17 % (from 9.11% to 10.16% for the champion devices). It is noteworthy that with the incorporation of the MNC buffer layer, series resistance (R_s) increased from 96 Ω to 103 Ω whereas the shunt resistance (R_{sh}) improved from 22.40 kΩ to 26.18 kΩ which indicates that the MNC buffer layer decreases current leakage at the heterojunction interface. The decrease of leakage current and the improvement of V_{OC} reflects also on the dark current- voltage analysis as shown in Figure 1(c). V_{OC} of the solar cell can be expressed as, $V_{OC} \approx \frac{\eta kT}{q} \ln(\frac{J_{ph}}{J_0})$. Where $\boldsymbol{\eta}$ is the diode ideality factor, J_0 is the reverse saturation current density and J_{ph} is the photo-generated current density. Decrease of J_0 is observed with MNC buffer layer incorporation which indicates the reduction leakage current and slight increase in V_{OC}. The decrease in calculated $\boldsymbol{\eta}$ (1.64 to 1.55 with MNC layer incorporation) from the dark current also indicates the reduction of interfacial recombination in the device. We have further performed Mott-Schottky analysis of capacitance-voltage (C-V) of our devices in an attempt to understand how the MNC buffer layer impacts the built-in potential (V_{bi}) and other characteristic of the heterojunction. Supporting Figure S3 shows the $1/C^2$-V measurements (and respective linear fits) of the devices. From there we extrapolate that the MNC buffer layer improves V_{bi} from 0.63 V to 0.68 V. The improved V_{bi} allows for more efficient charge transfer and charge collection.

J_{SC} improves with the addition of the MNC layer because the latter improves charge collection. To verify this, we investigated the external quantum efficiency (EQE) of the devices with and without an electrical bias. In accordance to previous reports, the external bias is set to the value corresponding to the maximum power point (MPP) of the device [24]. The EQE spectra without an applied bias are shown in Figure 2(a). These confirm that MNC incorporation improves the devices´ J_{SC} as the integrated J_{SC} from EQE spectra for MNC buffer layer is 21.7 mA/cm^2 compared to 19.8 mA/cm^2 of reference device. We attribute the apparent change in the shape of EQE spectrum between these two devices to the interference peak shift with the

optical thickness change due to the incorporation of MNC layer. The EQE spectra for the MPP points of the devices are shown in Figure 2(b). The integrated J_{SC} from EQE for reference showed much degraded value of 13.7 mA/cm^2 compared to 19.4 mA/cm^2 for the MNC buffer layer incorporated device. The difference between the EQE of reference and MNC layer incorporated devices with and without MPP-bias are shown in Figure 2(c), where we observe that this difference is increased when the MNC buffer layer is present. This confirms that the MNC buffer layer reduces interfacial recombination and enhances charge carrier collection efficiency even under low built-in electric field of the junction, as is the case under the MPP condition. Moreover, the screening of MNC layer over the ZnO has a significant effect on the hysteresis of the I-V curve. Supporting Figure S4 (a) & (b) show the hysteresis behaviour of the I-V curves for reference and MNC interface devices. It is observed that the MNC buffer layer dramatically decreases hysteresis. This can be attributed to the fact that the charge accumulation and transfer at the heterojunction with different voltage bias is influenced by the presence of interfacial traps[25]. The presence of such traps result in accumulation of photo-generated carrier at the heterojunction interface which subsequently cause significant hysteresis during the J-V scan. This charge accumulation and associated hysteresis is greatly suppressed by inserting the MNC layer.

We have also investigated the effect of MNC buffer layer on the stability of the cells. Figure 3 illustrates the evolution of different PV parameters for reference device and the MNC buffer layer inserted device (champion devices in both cases) up to 40 days stored and measured in ambient conditions. For both cases, V_{OC} and J_{SC} increased with time and then saturated similar to the earlier reported results[4]. Interestingly, the FF of the reference device decreased with time contrary to the MNC buffer layer inserted device which demonstrates a remarkably stable FF. Overall, the efficiency of the reference device slightly decreased after 40 days whereas the buffer layer improves the stability as shown in Figure 3(d). The major

reason for this improvement attributed to the stable value of FF over the course of the period. The insertion of the buffer layer at the heterojunction reduced recombination induced leakage and hence improve FF. This also supports previously explained reduction of hysteresis loss and field induced interfacial recombination.

We sought to further understand the effect of MNC buffer layer on charge collection and recombination. Intensity (Φ) dependent photocurrent (J_{ph}) variation shows that both reference and MNC devices have linear power dependency ($J_{ph} \propto \Phi^{p}$, $p = 1$) (Figure 4(a)). The diode ideality factor ($\boldsymbol{\eta}$) of the devices is estimated from the intensity dependent V_{OC} relation, $V_{OC} \approx \frac{\eta kT}{q}\ln(\Phi)$, where kT is the thermal energy and q is the elementary charge (Figure 4(b)). The estimated $\boldsymbol{\eta}$ for the reference device is 1.51 which is consistent with previously reported PbS QD based depleted heterojunction solar cells. $\boldsymbol{\eta}$ close to 1 indicates the transition into band to band recombination regime whereas $\boldsymbol{\eta}$ in between 1 and 2 indicates trap induced recombination[26]. Inserting the MNC layer reduced the value of $\boldsymbol{\eta}$ to 1.38. This reduction in $\boldsymbol{\eta}$ follows a similar trend in the aforementioned dark current method which indicates the reduction of interfacial recombination with the buffer layer.

The charge carrier recombination dynamics of the solar cells were further investigated with combined transient photo-voltage (TPV) and photocurrent (TPC) measurements. Recombination lifetime ($\boldsymbol{\tau}_r$) was calculated from an exponential fit on the photo-voltage transient curve. The TPV and TPC plot for both devices at a V_{OC} bias of 0.41 V is shown in Supporting Figure S5. The variation of $\boldsymbol{\tau}_r$ with V_{OC} is plotted in Figure 4(c) and it shows that the recombination is slowed by the addition of the MNC buffer layer. Moreover, the photo-generated charge carriers are estimated by combining TPV and TPC data[26-29] and this information is used for calculating the recombination rate by dividing the charge density by

recombination lifetime as depicted in Figure 4(d). Therein it is evident that the MNC interface device benefits from a lower recombination rate in agreement with our original hypothesis.

Conclusions:

We have shown that the insertion of a thin ZnO/PbS QD MNC layer acts as an efficient interfacial buffer layer in ZnO/ PbS heterojunction solar cells. Various device characterization measurements confirm the effectiveness of the MNC buffer layer for supressing interface recombination, improving charge collection at the respective side of the heterojunction, and ultimately for improving all the photovoltaic figures of merit of the solar cells. The improved photovoltaic performance and stability of the devices, combined with the simple solution processibility of the MNC buffer layer, renders this concept an attractive option to be considered for improving various other types of nanostructured heterojunction solar cells.

Acknowledgements

We acknowledge financial support from the European Research Council (ERC) under the European Union's Horizon 2020 research and innovation programme (grant agreement No 725165), the Spanish Ministry of Economy and Competitiveness (MINECO) and the "Fondo Europeo de Desarrollo Regional" (FEDER) through grant MAT2014-56210-R. This work was also supported by AGAUR under the SGR grant (2014SGR1548) and by European Union H2020 Programme under grant agreement n°696656 Graphene Flagship. We also acknowledge financial support from Fundacio Privada Cellex, the CERCA Programme and the Spanish Ministry of Economy and Competitiveness, through the "Severo Ochoa" Programme for Centres of Excellence in R&D (SEV-2015-0522).

Supporting information:

Experimental details; MNC layer thickness optimization; FIB SEM device micrograph; C-V analysis; Hysteresis of the J-V plots; TPV & TPC plots.

References:

(1) Carey, G. H.; Abdelhady, A. L.; Ning, Z.; Thon, S. M.; Bakr, O. M.; Sargent, E. H. Colloidal Quantum Dot Solar Cells. *Chem. Rev.* **2015**, *115*, 12732–12763.

(2) Sargent, E. H. Colloidal Quantum Dot Solar Cells. *Nat. Photonics*, **2012**, *6*, 133-135.

(3) Nozik, A. J.; Beard, M. C.; Luther, J. M.; Law, M.; Ellingson, R. J.; Johnson, J. C. Semiconductor Quantum Dots and Quantum Dot Arrays and Applications of Multiple Exciton Generation to Third-Generation Photovoltaic Solar Cells. *Chem. Rev.* **2010**, *110*, 6873–6890.

(4) Chuang, C.-H. M.; Brown, P. R.; Bulović, V.; Bawendi, M. G. Improved performance and stability in quantum dot solar cells through band alignment engineering. *Nat. Mater.* **2014**, *13*, 796– 801.

(5) Kagan, C. R.; Lifshitz, E.; Sargent, E. H.; Talapin, D. V. Building Devices from Colloidal Quantum Dots. *Science*, **2016**, *353*, 885.

(6) Jeong, K.S; Tang, J.; Liu, H.; Kim, J.; Schaefer, A. W; Kemp, K.; Levina, L.; Wang, X.; Hoogland, S.; Debnath, R.; Brzozowski, L.; Sargent, E. H.; Asbury, J. B. Enhanced Mobility-Lifetime Products in PbS Colloidal Quantum Dot Photovoltaics. *ACS Nano*, **2012**, *6*, 89-99.

(7) Brown, P. R., Kim, D.; Lunt, R. R.; Zhao, N.; Bawendi, M. G.; Grossman, J. C.; Bulovic, V. Energy Level Modification in Lead Sulfide Quantum Dot Thin Films through Ligand Exchange. *ACS Nano,* **2014**, *8*, 5863-5872.

(8) McDonald, S. A.; Konstantatos, G; Zhang, S.; Cyr, P. W.; Klem, E.J.D.; Levina, L.; Sargent, E.H. Solution-Processed PbS Quantum Dot Infrared Photodetectors and Photovoltaics. *Nat. Mater.* **2005**, *4*, 138-142.

(9) Liu, M.; Voznyy, O.; Sabatini, R.; Garcia de Arquer, F. P.; Munir, R.; Balawi, A. H.; Lan, X.; Fan, F.; Walters, G.; Kirmani, A. R.; Hoogland, S.; Laquai, F.; Amassian, A; Sargent, E. H. Hybrid Organic–Inorganic Inks Flatten the Energy Landscape in Colloidal Quantum Dot Solids. *Nat. Mater.* **2017**, *16*, 258-263.

(10) Chuang, C.-H. M.; Maurano, A.; Brandt, R. E.; Hwang, G. W.; Jean, J.; Buonassisi, T; Bulović, V.; Bawendi, M. G. Open-Circuit Voltage Deficit, Radiative Sub-Bandgap States, and Prospects in Quantum Dot Solar Cells. *Nano Lett.*, **2015**, *15*, 3286–3294.

(11) Stavrinadis, A.; Pradhan, S.; Papagiorgis, P.; Itskos, G.; Konstantatos, G. Suppressing Deep Traps in PbS Colloidal Quantum Dots via Facile Iodide Substitutional Doping for Solar Cells with Efficiency >10%. *ACS Energy Lett.* **2017**, *2*, 739−744.

(12) Pradhan, S.; Stavrinadis, A.; Gupta, S.; Bi, Y.; Di Stasio, F.; Konstantatos, G. Trap-State Suppression and Improved Charge Transport in PbS Quantum Dot Solar Cells with Synergistic Mixed-Ligand Treatments. *Small*, **2017** (DOI: 10.1002/smll.201700598).

(13) Byers, J. C.; Ballantyne, S.; Rodionov, K.; Mann, A.; Semenikhin, O. A. Mechanism of Recombination Losses in Bulk Heterojunction P3HT:PCBM Solar Cells Studied Using Intensity Modulated Photocurrent Spectroscopy. *ACS Appl. Mater. Interfaces* **2011**, *3*, 392–401.

(14) Tan, F.; Wang, Z.; Qu, S.; Cao, D.; Liu, K.; Jiang, Q.; Yang, Y.; Pang, S.; Zhang, W.; Lei, Y.; Wangb, Z. A CdSe Thin Film: A Versatile Buffer Layer for Improving the Performance of TiO_2 Nanorod Array: PbS Quantum Dot Solar Cells. *Nanoscale*, **2016**, *8*, 10198-10204.

(15) Kemp, K. W.; Labelle, A. J.; Thon, S. M.; Ip, A. H.; Karmer, I. J.; Hoogland, S.; Sargent, E. H. Interface Recombination in Depleted Heterojunction Photovoltaics based on Colloidal Quantum Dots. *Adv. Energy. Mater.* **2013**, *3*, 917-922.

(16) Chang, J.; Kuga, Y.; Mora-Seró, I.; Toyoda, T.; Ogomi, Y.; Hayase, S.; Bisquert, J.; Shen, Q. High Reduction of Interfacial Charge Recombination in Colloidal Quantum Dot Solar Cells by Metal Oxide Surface Passivation. *Nanoscale*, **2015**, *7*, 5446–5456.

(17) Yuan, M.; Voznyy, O.; Zhitomirsky, D.; Kanjanaboos, P.; Sargent, E. H. Synergistic Doping of Fullerene Electron Transport Layer and Colloidal Quantum Dot Solids Enhances Solar Cell Performance. *Adv. Mater.* **2015**, *27*, 917-921.

(18) Zhang, X.; Johansson, E. M. J. Reduction of Charge Recombination in PbS Colloidal Quantum Dot Solar Cells at the Quantum Dot/ZnO Interface by Inserting a MgZnO Buffer Layer. *J. Mater. Chem. A*, **2017**, *5*, 303-310.

(19) Ehrler, B.; Musselman, K. P.; Böhm, M. L.; Morgenstern, F. S. F.; Vaynzof, Y.; Walker, B. J.; MacManus-Driscoll, J. L.; Greenham, N. C. Preventing Interfacial Recombination in Colloidal Quantum Dot Solar Cells by Doping the Metal Oxide. *ACS Nano*, **2013**, *7*, 4210–4220.

(20) Zhao, T.; Goodwin, E. D.; Guo, J; Wang, H.; Diroll, B. T.; Murray, C. B; Kagan, C. R. Advanced Architecture for Colloidal PbS Quantum Dot Solar Cells Exploiting a CdSe Quantum Dot Buffer Layer. *ACS Nano*, **2016**, *10*, 9267–9273.

(21) Rath, A. K.; Garcia de Arquer, F. P.; Stavrinadis, A.; Lasanta, T.; Bernechea, M.; Diedenhofen, S. L.; Konstantatos, G. Remote Trap Passivation in Colloidal Quantum Dot Bulk Nano-heterojunctions and Its Effect in Solution-Processed Solar Cells. *Adv. Mater.* **2014**, *26*, 4741– 4747.

(22) Pradhan, S.; Stavrinadis, A.; Gupta, S.; Christodoulou, S.; Konstantatos, G. Breaking the Open-circuit Voltage Deficit Floor in PbS Quantum Dot Solar Cells Through Synergistic Ligand and Architecture Engineering, *ACS Energy Lett.* **2017,** *2***,** 1444 – 1449.

(23) Cao, Y.; Stavrinadis, A.; Lasanta, T.; So, D.; Konstantatos, G. The Role of Surface Passivation for Efficient and Photostable PbS Quantum Dot Solar Cells. *Nat. Energy*, **2016**, *1*, 16035.

(24) Liu, M.; García de Arquer, F. P.; Li, Y.; Lan, X.; Kim, G.; Voznyy, O.; Jagadamma, L. K.; Abbas, A. S.; Hoogland, S.; Lu, Z.; Kim, J. Y.; Amassian, A.; Sargent, E. H. Double-Sided Junctions Enable High-Performance Colloidal-Quantum-Dot Photovoltaics. *Adv. Mater.* **2016,** *28*, 4142-4148.

(25) Kim, H.-S.; Jang, I.-H.; Ahn, N.; Choi, M.; Guerrero, A.; Bisquert, J.; Park, N.-G. Control of I–V Hysteresis in $CH_3NH_3PbI_3$ Perovskite Solar Cell. *J. Phys. Chem. Lett.* **2015**, *6*, 4633−4639.

(26) Zhao, N.; Osedach, T. P.; Chang, L.-Y.; Geyer, S. M.; Wanger, D.; Binda, M. T.; Arango, A. C.; Bawendi, M. G.; Bulovic, V. Colloidal PbS Quantum Dot Solar Cells with High Fill Factor. *ACS Nano*, **2010**, *4*, 3743-3752.

(27) Shuttle, C. G.; O'Regan, B.; Ballantyne, A. M.; Nelson, J; Bradley, D. D. C; de Mello, J; Durrant, J. R. Experimental Determination of the Rate Law for Charge Carrier Decay in a Polythiophene: Fullerene Solar Cell. *Appl. Phys. Lett.*, **2008**, *92*, 093311.

(28) Chang, J.; Kuga, Y.; Mora-Seró, I.; Toyoda, T.; Ogomi, Y.; Hayase, S.; Bisquert, J.; Shen, Q. High Reduction of Interfacial Charge Recombination in Colloidal Quantum Dot Solar Cells by Metal Oxide Surface Passivation, *Nanoscale*, **2015**, *7*, 5446-5456.

(29) Zaban, A.; Greenshtein, M.; Bisquert, J. Determination of the Electron Lifetime in Nanocrystalline Dye Solar Cells by Open-Circuit Voltage Decay Measurements, *Chem. Phys. Chem.*, **2003**, *4*, 859-864.

Device	V_{OC} *(V)*	J_{SC} *(mA/cm^2)*	*FF*	*Efficiency (%)*	R_s *(Ω)*	R_{sh} *(kΩ)*
Reference	0.593±.005 (0.60)	23.26±0.30 (23.54)	0.640±0.011 (0.65)	8.80±0.24 (9.11)	96±14 (99)	21.00±2.73 (22.40)
With MNC interface	0.605±.005 (0.61)	25.06±0.13 (25.23)	0.651±.005 (0.66)	9.87±0.17 (10.16)	103±5 (96)	25.33±2.54 (26.18)

Table 1: Summary of photovoltaic figures of merit for Reference PbS QD based and MNC interfacial buffer layer incorporated devices (average over 6 devices for each case). The values in brackets indicate the champion device.

Figures:

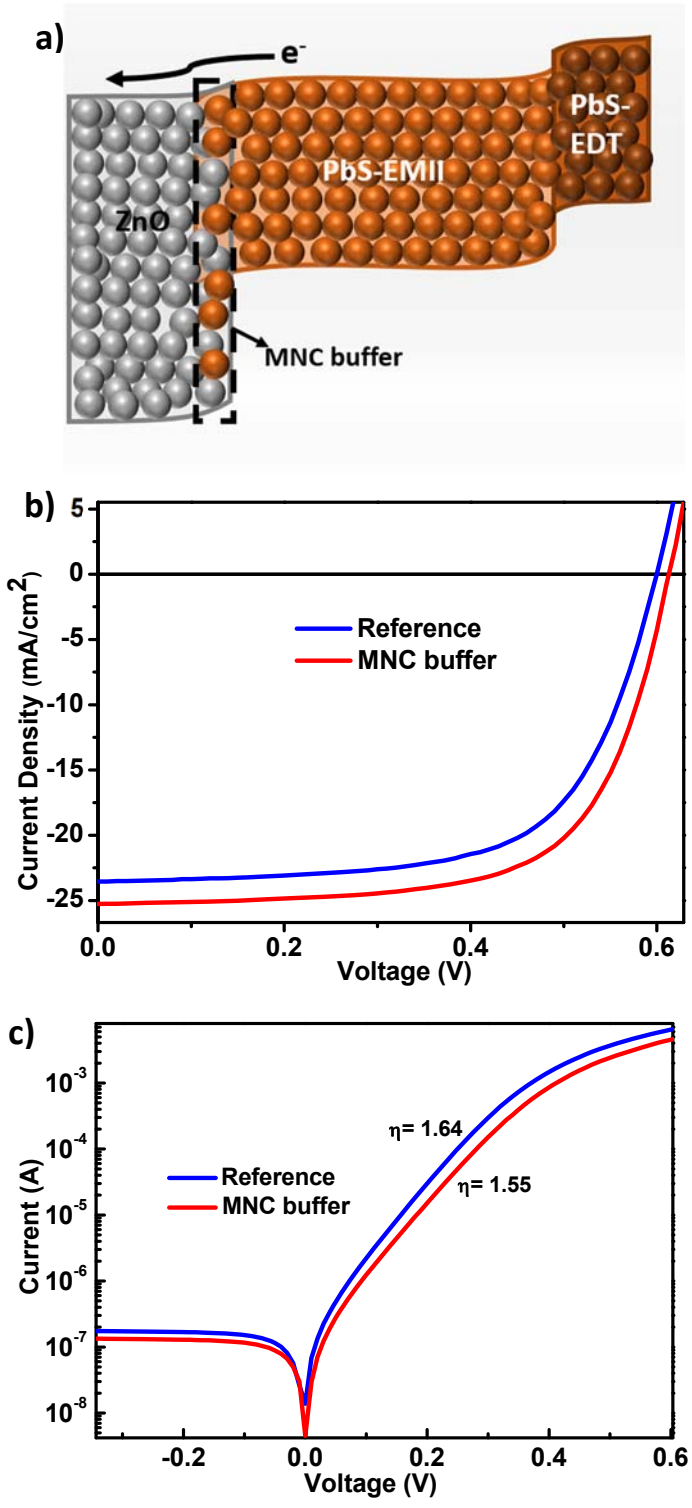

Figure 1: (a) Schematic energy band alignment of the device with inserting MNC layer in short-circuit condition. The MNC layer facilitated electron transport and increases charge collection efficiency. (b) Photovoltaic performance of Reference and MNC buffer layer based device. (c) Dark current of Reference and MNC buffer layer inserted device.

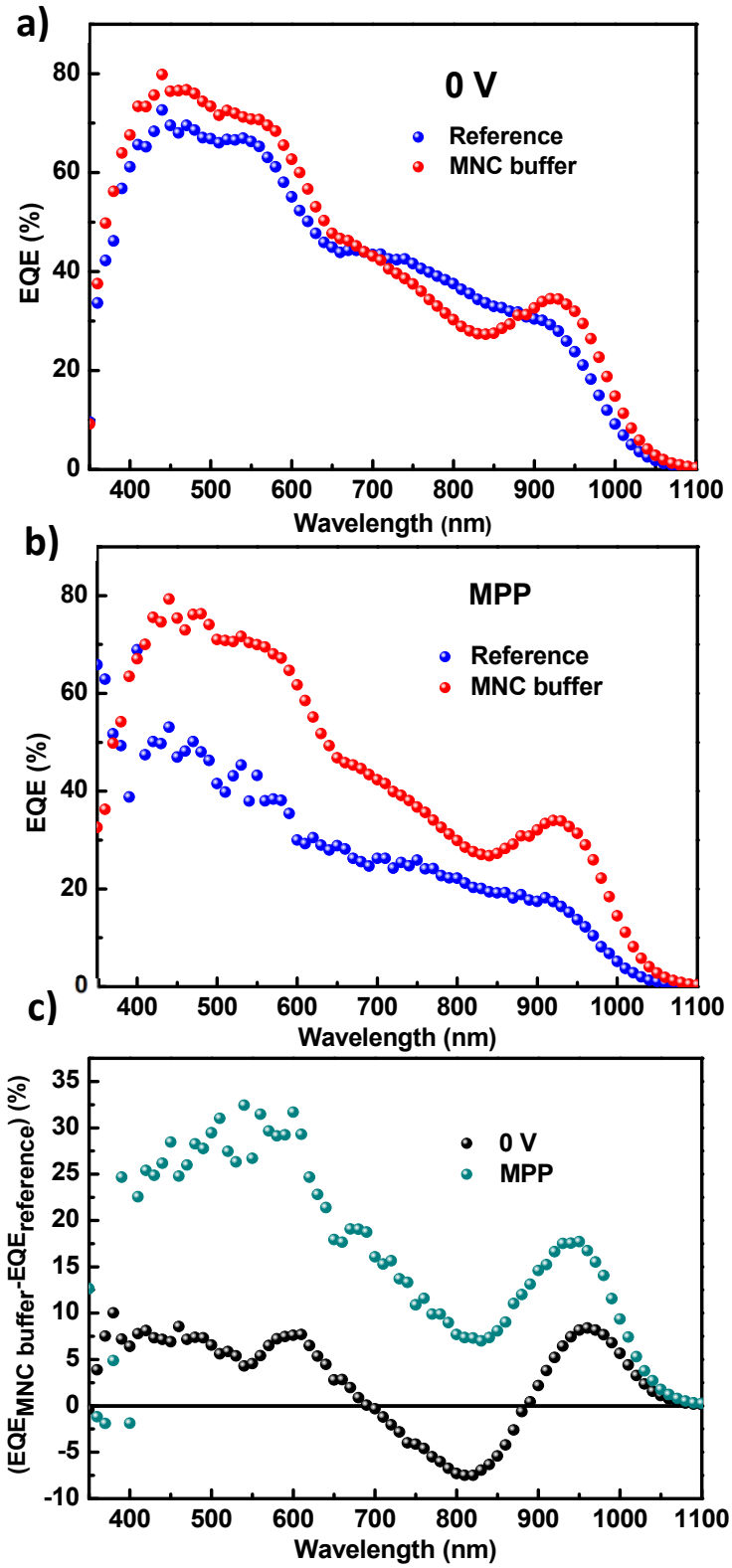

Figure 2: EQE spectra for both devices at (a) 0 V and (b) at MPP (maximum power point) bias. (c) Spectral EQE difference between reference and MNC buffer layer-device at 0 V and MPP. Voltage bias dependence of charge collection is less effective with MNC buffer layer incorporation.

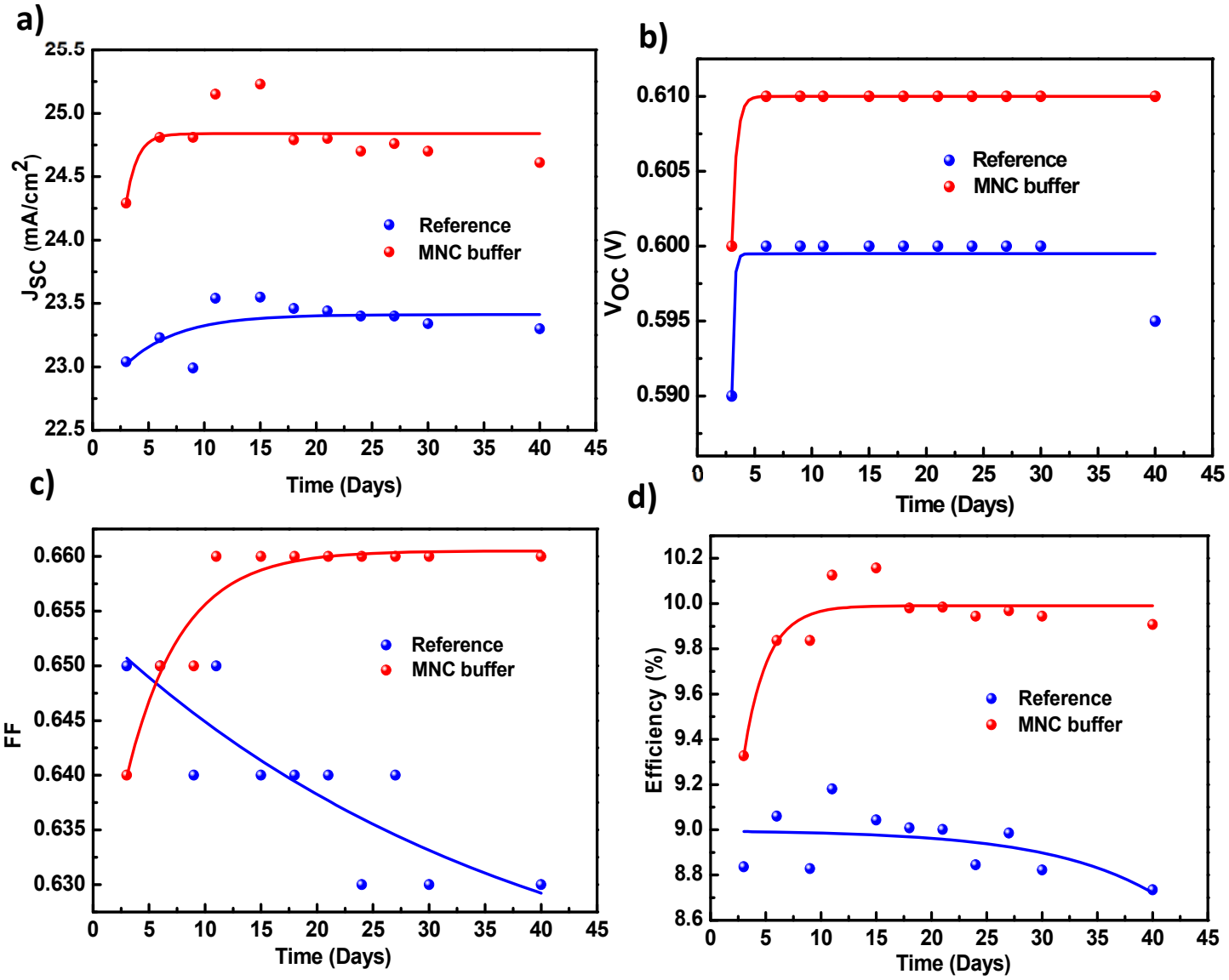

Figure 3: Comparison of the evolution of PV parameters ((a) J_{SC}, (b) V_{OC}, (c) FF, (d) Efficiency) between reference and MNC buffer layer inserted devices (champion devices in both cases) up to 40 days stored in ambient condition.

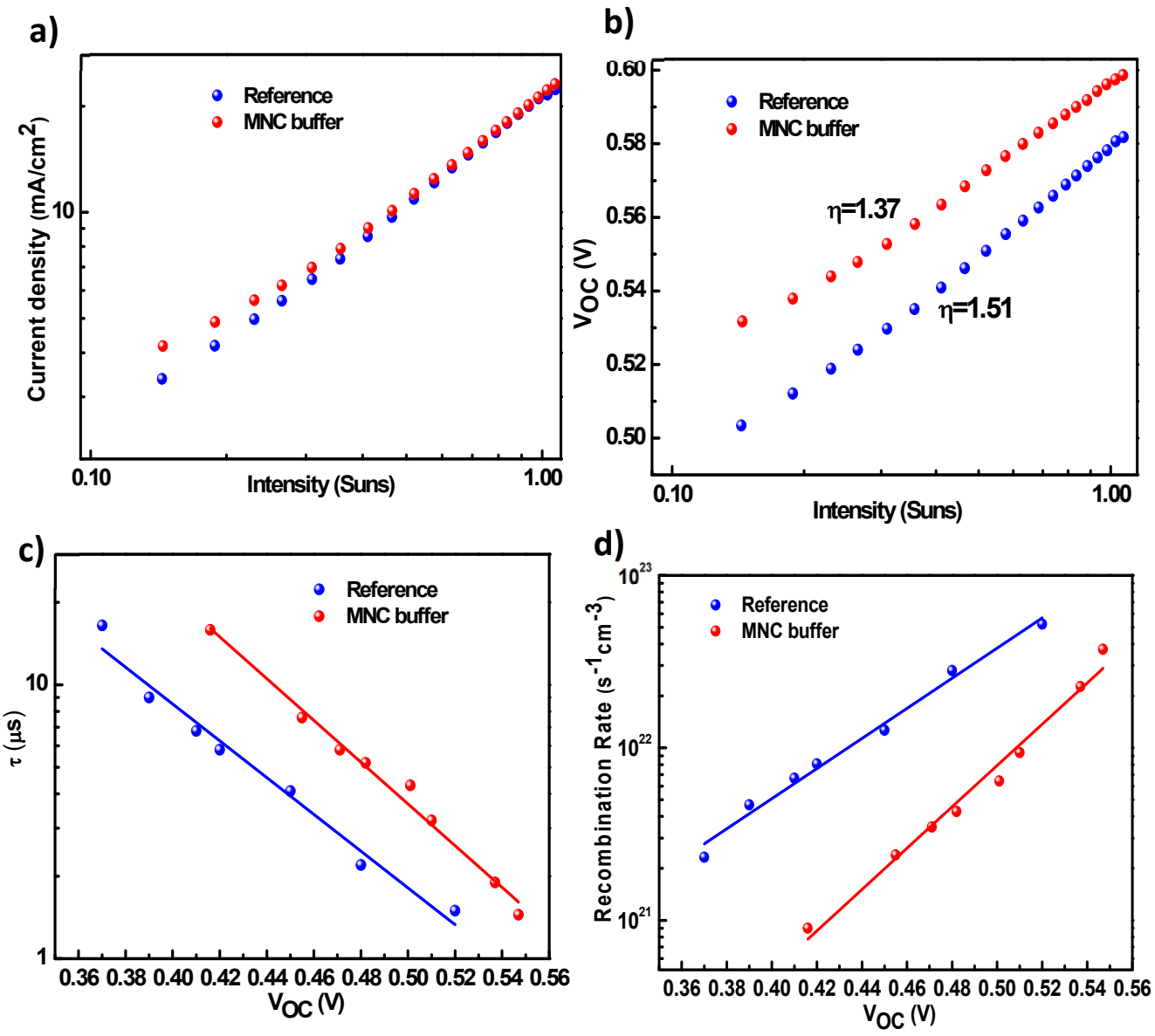

Figure 4: Intensity dependent (a) photocurrent and (b) V_{OC} variation for Reference and MNC interface devices. (c) Comparison of recombination lifetime (τ_r) (d) Recombination rate (R) for both devices.

TOC:

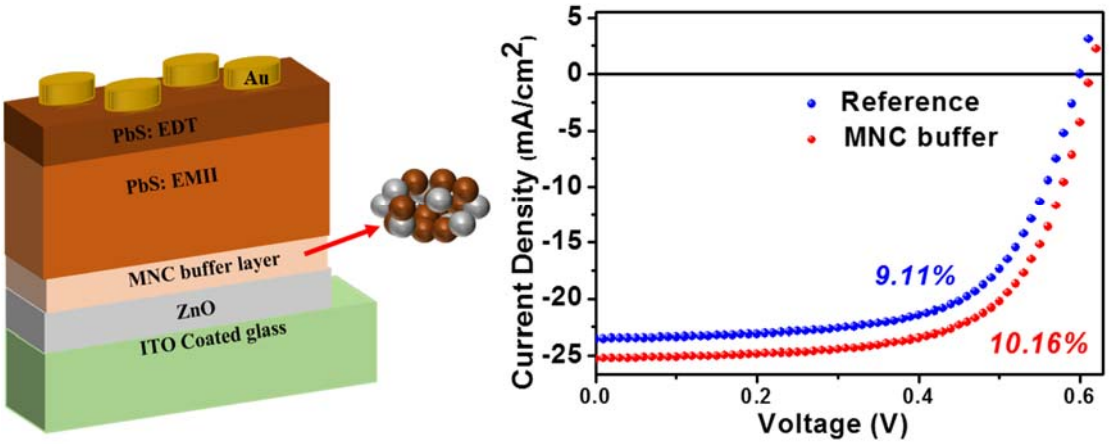
Au
PbS: EDT
PbS: EMII
MNC buffer layer
ZnO
ITO Coated glass
Current Density (mA/cm2)
Voltage (V)
Reference
MNC buffer
9.11%
10.16%
5
0
-5
-10
-15
-20
-25
0.0
0.2
0.4
0.6